www.reading.ac.uk/centaur

CentAUR

Central Archive at the University of Reading

Reading's research outputs online

Crystallization and Stereocomplexation Behavior of Poly(D- and L-lactide)-*b*-poly(*N*,*N*-dimethylamino-2-ethyl methacrylate) Block Copolymers

Rose Mary Michell,[1] Alejandro J. Müller,[1] Mariya Spasova,[2] Philippe Dubois[2],*

Stefano Burattini[3], Barnaby W. Greenland[3], Ian W. Hamley [3], Daniel Hermida-Merino[4]

Nicolas Cheval[5], Amir Fahmi[5]

1 Grupo de Polímeros USB, Departamento de Ciencia de los Materiales, Universidad Simón Bolívar, Apartado 89000, Caracas 1080-A, Venezuela

2 Laboratory of Polymeric and Composite Materials, Center of Innovation and Research in Materials & Polymers (CIRMAP), University of Mons-Hainaut, Place du Parc 20, Mons B-7000, Belgium

3 Department of Chemistry, University of Reading, Reading RG6 6AD, United Kingdom

4 ESRF, 6 rue Jules Horowitz, BP 220, Grenoble 38043 Cedex 9, France

5 Department of Mechanical, Materials and Manufacturing Engineering, University of Nottingham, University Park, NG7 2RD Nottingham, UK

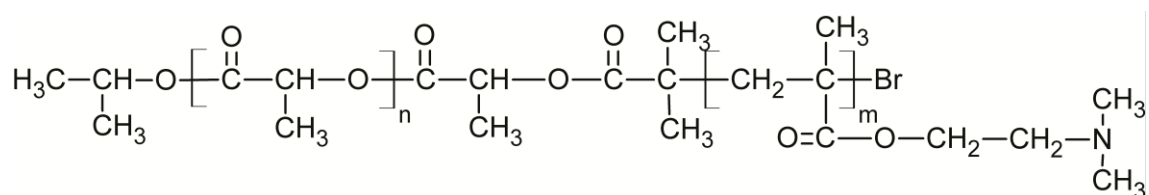*Corresponding author: amuller@usb.ve

ABSTRACT

The thermal properties, crystallization and morphology of amphiphilic poly(D-lactide)-*b*-poly(*N*,*N*-dimethylamino-2-ethyl methacrylate) (PDLA-*b*-PDMAEMA) and poly(L-lactide)-*b*-poly(*N*,*N*-dimethylamino-2-ethyl methacrylate) (PLLA-*b*-PDMAEMA) copolymers were studied and compared to that of the corresponding poly(lactide) homopolymers. Additionally, stereocomplexation of these copolymers was studied. The crystallization kinetics of the PLA blocks was retarded by the presence of the PDMAEMA block. The studied copolymers were found to be miscible in the melt and the glassy state. The Avrami theory was able to predict the entire crystallization range of the PLA isothermal overall crystallization. The melting points of PLDA/PLLA and PLA/PLA-*b*-PDMAEMA stereocomplexes were higher than those formed by copolymer mixtures. This indicates that the PDMAEMA block is influencing the stability of the stereocomplex structures. For the low molecular weight samples, the stereocomplexes particles exhibited a conventional disk-shape structure and, for high molecular weight samples, the particles displayed unusual star-like shape morphology.

KEYWORDS: *Poly(lactic acid) (PLA) copolymers, isothermal crystallization kinetics, stereocomplexes, crystallization in block copolymers.*

INTRODUCTION

Poly(lactide) (PLA) polymers are promising new biocompatible and biodegradable materials. Poly(lactides) can be obtained from annually renewable resources and represent interesting materials to replace petroleum-based polymers.[1,2] PLA has three different stereoisomers: poly(L-lactic acid), poly (D-lactic acid) and racemic poly(D,L-lactic acid). The first two are semicrystalline and the last one is amorphous.[3] In 1987 Ikada et al. reported the phenomenon of stereocomplexation between optically active poly(L-lactic acid) (PLLA) and poly(D-lactic acid) (PDLA) homopolyesters. [4,5] The PLA stereocomplexes have melting temperatures around 220-230 °C compared to about 170-180 °C for the homopolymers. The PLA stereocomplexes have a higher mechanical and thermal resistance than the homopolymers. These characteristics motivate further research into stereocomplexation phenomena. [6]

On the other hand, the poly(*N,N*-dimethylamino-2-ethyl methacrylate) (PDMAEMA) homopolymer is amorphous and has been used widely in the biomedical field. The PDMAEMA homopolymer has antibacterial, hemostatic and anticancer properties. [7,8] The synthesis of the PLA-*b*-PDMAEMA copolymers (see scheme 1) has been inspired by potential applications in the biomedical materials field [9,10].

Scheme 1. Schematic representation of the structure of PLA-*b*-PDMAEMA diblock copolymer.

The synthesis of these copolymers has been previously reported [9]. The copolymers were synthesized in three steps, the first one is the controlled ring-opening polymerization of

the D-lactide or L-lactide using as initiator aluminum triisopropoxide (Al(OiPr)$_3$). In the second step PLA-OH is transformed into PLA-Br, finally the PLA-Br was used as a macroinitiator for the ATRP polymerization of the DMAEMA.

The crystallization of block copolymers has been an active area of research for the past several decades. The influence of the microphase separation in the crystallization of the blocks has been studied [11-13]. In the case of the PLA-*b*-PDMAEMA block copolymers only one of the blocks can crystallize, i.e., PLA. The crystallization of PLA is interesting since it can exhibit cold crystallization phenomena, its crystallization kinetics is largely dependent on the molecular weight and it can form three different crystalline unit cells (α, β, γ).[6,14-20]

The thermal properties are very important for the determination of the final application of a thermoplastic polymer. Additionally if the polymers are semicrystalline the study of the crystallization kinetics is indispensable. In this publication we perform a comprehensive study on the morphology, nucleation, isothermal crystallization and visualisation of stereocomplex structures of several PLA-*b*-PDMAEMA block copolymers.

EXPERIMENTAL PART

Materials

The characteristics of the employed materials are shown in Table 1, the nomenclature used is as follows: D(L)L$_{xx}$-b-DMAEMA$_{yy}^{zz}$, where *xx* and *yy* represent the content (in weight percent) of the PLA and PDMAEMA blocks respectively. The superscript *zz* represents the number-average molecular weight in kg/mol. The complete synthesis procedure of all studied block copolymers has been already reported by some of us. [9]

Table 1. Molecular characteristics of the PLA-*b*-PDMAEMA block copolymers

Nomenclature	Type	M_n (g/mol)	PI*	PDLA (wt %)	PLLA (wt %)	PDMAEMA (wt %)
DL$_{100}^{4.2}$	Homopolymer	4180	1.15	100		0
LL$_{100}^{4.2}$	Homopolymer	4220	1.16		100	0
DL$_{45}$-b-MA$_{55}^{9.2}$	Copolymer	9210	1.39	45		55
LL$_{44}$-b-MA$_{56}^{9.7}$	Copolymer	9560	1.42		44	56
DL$_{100}^{10.4}$	Homopolymer	10350	1.4	100		
LL$_{100}^{10.5}$	Homopolymer	10500	1.26		100	
DL$_{65}$-b-MA$_{35}^{15.9}$	Copolymer	15850	1.46	65		35
LL$_{64}$-b-MA$_{36}^{16.5}$	Copolymer	16500	1.36		64	36

*Number-average molecular weight of PLA block and polydispersity index (PI, $\overline{M}_W / \overline{M}_n$) of the copolymers as determined by SEC in THF using PS standards for calibration.

Standard DSC experiments

A Perkin-Elmer Pyris 1 differential scanning calorimeter was used for the thermal analysis of the copolymers. The samples were studied under inert atmosphere employing ultrapure nitrogen. The weight of the samples was about 5 mg and the scanning rate was 20°C/min during cooling and heating. The thermal history was erased keeping the sample at a high temperature (at the peak melting point plus 20°C) for 3 min.

Isothermal Crystallization

The first step was to erase the thermal history, after that the samples were cooled from the melt at 60 °C/min to a defined crystallization temperature. The crystallization exotherm was recorded as a function of time until saturation was reached (at approximately three times the half-crystallization time). Then the sample was heated at 20 °C/min in order to examine the melting behavior of the isothermally crystallized copolymer. A T_c range of at least 7 different temperatures was employed. The samples were very sensitive to thermal degradation. Therefore, for each isothermal temperature investigated, a new DSC pan with fresh sample was employed to avoid the influence of degradation on the results. [21]

Wide and Small Angle X-ray Scattering (WAXS AND SAXS)

Small- and wide-angle X-ray scattering (SAXS and WAXS) experiments were performed on station BM26B (DUBBLE), ESRF, Grenoble, France. A modified DSC Linkam hot stage was employed that allows the transmission of X-rays through mica windows. At first

the sample was heated from 25°C to 110 °C at 20 °C/min, after that the sample was again heated at 20°C/min to 175 °C. After 5 minutes the samples were cooled at 5 °C/min to 25 °C. The wavelength employed was $\lambda=1.24$Å and the sample-detector distance was 3.75 m. The wavenumber $q = 4\pi \sin \theta/\lambda$ scale for SAXS was calibrated using collagen and NBS silicon.

Atomic Force Microscopy

Topographic images of the surfaces of thin films were obtained via atomic force microscopy under Tapping Mode^{TM} at ambient conditions, using a Dimension IVa Nanoscope (Digital Instruments). Standard silicon cantilevers were used, with a resonance frequency of about 330 kHz, a spring constant of 45 N m^{-1} and a tip radius of less than 10 nm (Pointprobe SPM Cantilevers, Nanoworld). The operating frequency was chosen to be far on the repulsive side of the resonance frequency to increase scanning performance and stability.

Homopolymers and copolymers films were obtained by melting the sample on a glass substrate; later the sample was covered with *Kapton*® and another glass cover, then the film was cooled down at 5 ^{o}C/min to ambient temperature.

Scanning Electron Microscopy (SEM)

SEM was employed to observe the morphology of stereocomplexes. The samples were coated with an ultra fine layer of platinum. Then they were observed in a Philips XL30 ESEM FEG instrument at 20 kV.

Stereocomplex Preparation

Pairs of copolymers (Table 2) were dissolved into dichloromethane at room temperature. The solutions were formed using equimolar quantities of PLLA and PDLA, the concentration of the solutions was 1 wt%. Each component was dissolved separately and later the solutions were mixed for the sterocomplex formation. After complete dissolution, the dichloromethane was evaporated at room temperature and the stereocomplexes were obtained.

RESULTS AND DISCUSSION

Morphology

The morphology of a block copolymer determines the majority of the physical properties of the material. One of the most interesting characteristics of block copolymers is their ability to form microdomains. The formation of microdomains is dependent on the segregation strength and the composition of the copolymer. The parameter χN or segregation strength, where χ is the Flory-Huggins interaction parameter and N the degree of polymerization, is used to quantify microphase separation.

Table 2. Copolymer pairs employed to study stereocomplexes formation

Stereocomplex	L-lactide component	D-lactide component
Sc1	$LL_{100}^{4.2}$	$DL_{100}^{4.2}$
Sc2	$LL_{100}^{10.5}$	$DL_{100}^{10.4}$
Sc3	$LL_{44}\text{-}b\text{-}MA_{56}^{9.7}$	$DL_{45}\text{-}b\text{-}MA_{55}^{9.2}$
Sc4	$LL_{64}\text{-}b\text{-}MA_{36}^{16.5}$	$DL_{65}\text{-}b\text{-}MA_{35}^{15.9}$
Sc5	$LL_{44}\text{-}b\text{-}MA_{56}^{9.7}$	$DL_{100}^{4.2}$
Sc6	$LL_{100}^{4.2}$	$DL_{45}\text{-}b\text{-}MA_{55}^{9.2}$
Sc7	$LL_{64}\text{-}b\text{-}MA_{36}^{16.5}$	$DL_{100}^{10.4}$
Sc8	$LL_{100}^{10.5}$	$DL_{65}\text{-}b\text{-}MA_{35}^{15.9}$

The Flory-Huggins interaction parameter can be roughly estimated by equation 1 [22]

$$\chi = V_{seg}\frac{\left(\delta_{PLA} - \delta_{PDMAEMA}\right)^2}{RT} \tag{Eq 1}$$

where *Vseg* is the volume of a polymer segment, δ_{PLA} and $\delta_{PDMAEMA}$ are the solubility parameters for PLA and PDMAEMA respectively, *R* is the universal gas constant and *T* is the temperature. However, it is possible to obtain significantly different values of χ depending on the method used for the estimation of the solubility parameter for PDMAEMA homopolymer (since this value has not been determined experimentally and

must be calculated). We have employed the group contribution theory following Van Krevelen [22] in order to perform such approximate calculation. Estimated values of χN are shown in Table 3, they can only be considered a first order approximation.

Table 3. Estimated χN values for PLA-*b*-PDMAEMA block copolymers

Copolymer	χN
DL$_{45}$-*b*-MA$_{55}$$^{9.2}$	51
LL$_{44}$-*b*-MA$_{56}$$^{9.7}$	53
DL$_{65}$-*b*-MA$_{35}$$^{15.9}$	102
LL$_{64}$-*b*-MA$_{36}$$^{16.5}$	105

According to the values shown in Table 3, microphase separation would be expected since for symmetric diblock copolymers it has been calculated that the critical value of $\chi N =$ 10.5. [23,24]. As expected, the higher molecular weight samples have higher predicted segregation strengths. Nevertheless, these values may have a large error associated with them as explained above.

Figure 1 shows AFM images of samples prepared from the melt. These films have a thickness around 10 μm. When the film is thick there is no influence of the substrate on the morphology of the copolymer and the bulk-like behavior can be observed. If the segregation in the diblock copolymers is strong, spherulitic structures cannot be obtained, because the polymer crystallizes within a confined space. All samples in Figure 1 show morphological features resembling spherulites. This result can be explained by two possible arguments: (a) the block copolymers crystallize from a single phase melt (they are miscible

10

in the melt) or (b) the phase segregation between the copolymers is weak in the melt and upon cooling crystallization drives structure formation (a phenomenon that has been described in the literature as break-out [25]).
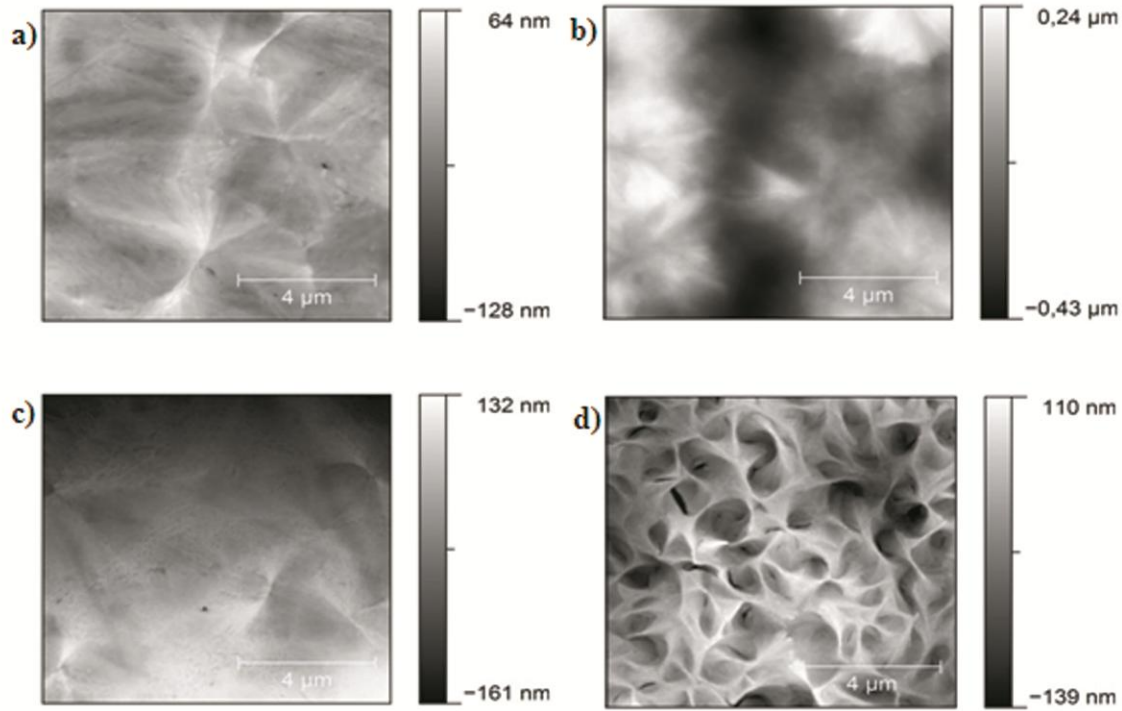

Figure 1. AFM height images of thick film obtained from the melt. a) DL_{45}-b-$DMAEMA_{55}^{9.6}$; b) LL_{44}-b-$DMAEMA_{56}^{9.6}$; c) DL_{65}-b-$DMAEMA_{35}^{15.9}$; d) LL_{64}-b-$DMAEMA_{34}^{16.5}$

The AFM results conclusively indicate that the PDMAEMA and PLA blocks are either miscible in the melt or at least weakly segregated (according to the spherulitic morphology), despite the values of χN presented in Table 3 that indicate medium or strong segregation [12,26] This disagreement could be due to the method employed to obtain the values of χN and the uncertainties regarding the value of the solubility parameter of PDMAEMA.

Key evidences to ascertain the structure of the melt can usually be obtained by Small Angle X-ray Scattering (SAXS). SAXS studies demonstrate that the blocks are miscible in the melt, for the LL copolymers, since no maximum in the SAXS profile (determined at a temperature where all samples are in the melt) was observed in Figure 2(a, c). However, for DL copolymers we were able to observe a weak maximum or shoulder in the SAXS data (see arrow in Figure 2(b, d)) that may indicate structural heterogeneity in the melt, however this evidence is not conclusive and should be compared with other results. In fact, as evidenced by AFM above and DSC below, the results are more consistent with miscibility between the block components.
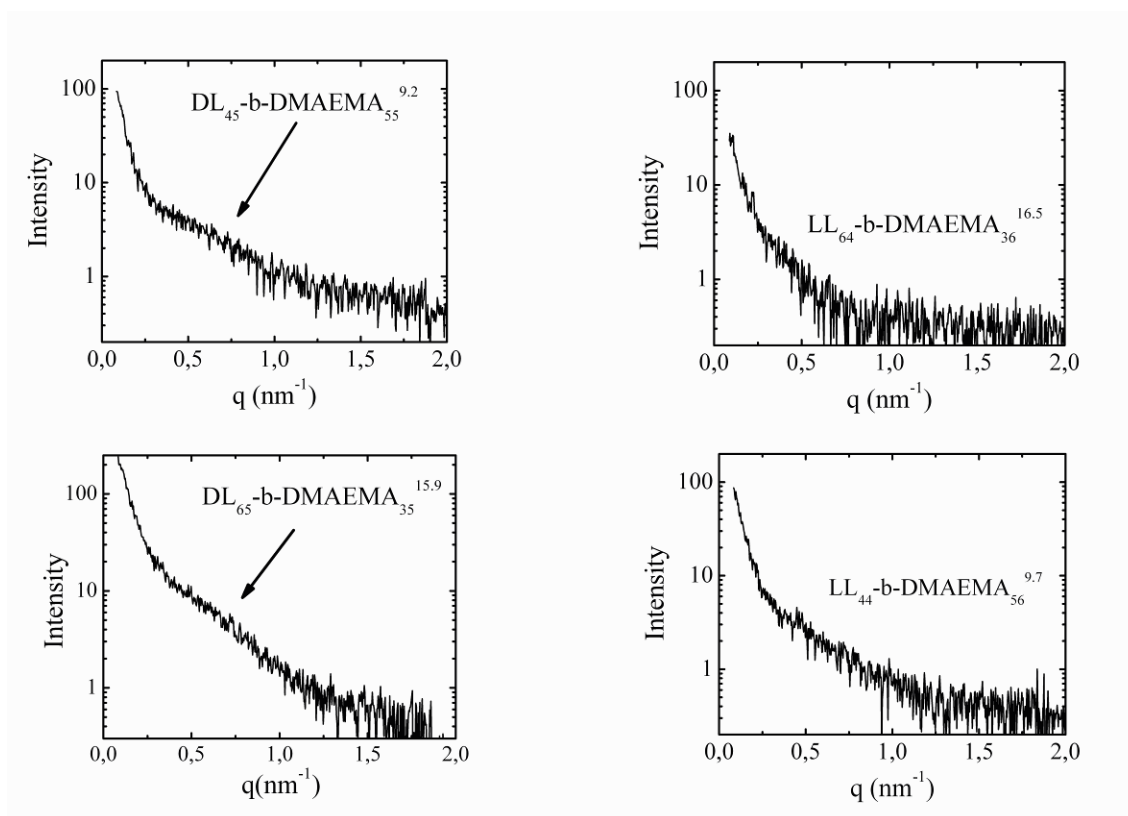

Figure 2. SAXS patterns obtained at 175 °C for the PLA-*b*-PDMAEMA copolymers.

WAXS results

PLA is the semi-crystalline block in the PLA-*b*-PDMAEMA block copolymers. PLA can crystallize in three different unit cells, α, β and γ. [6,16,27] According to the results shown in Figure 3 and Table 4, the crystalline unit cell for the PDLA and PLLA is the same in all homopolymers and copolymer samples irrespective of their stereo-regularity differences. The crystalline structure probably corresponds to the orthorhombic α unit cell, since the values of the reflections obtained (see Table 4) are much closer to those of the α form than β (and they are also different than the values for the unexpected γ). The α form is the most commonly formed for PLA during the crystallization from the melt or a dilute solution. [28]
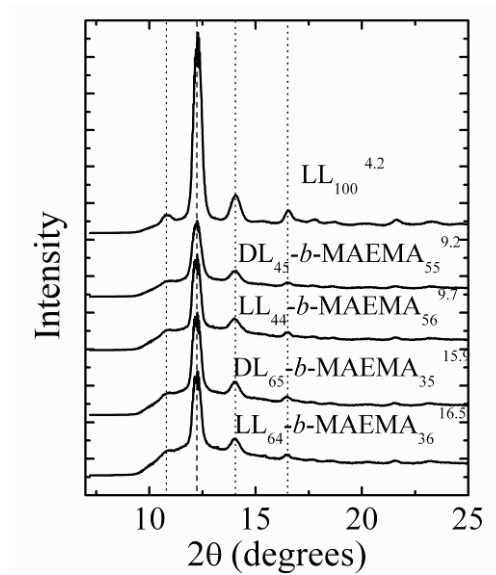

Figure 3. WAXS patterns obtained at 25 °C after controlled cooling from the melt (at 5 °C/min) for the samples indicated.

Table 4. WAXS reflections observed in Figure 3 and their interplanar distances. [28]

Samples	2θ (deg)/d(Å)				
$DL_{100}^{4.2}$	10.85/6.55	12.23/5.82	14.10/5.05	16.58/4.32	21.7/3.29
$LL_{100}^{4.2}$	10.81/6.58	12.28/5.80	14.04/5.09	16.53/4.31	21.64/3.30
$DL_{45}\text{-}b\text{-}MA_{55}^{9.2}$	10.77/6.60	12.23/5.82	13.99/5.07	16.53/4.31	21.64/3.30
$LL_{44}\text{-}b\text{-}MA_{56}^{9.7}$	10.82/6.57	12.23/5.82	14.04/5.09	16.43/4.33	21.64/3.30
$DL_{65}\text{-}b\text{-}MA_{35}^{15.9}$	10.82/6.57	12.18/5.84	14.04/5.07	16.48/4.33	21.55/3.32
$LL_{64}\text{-}b\text{-}MA_{36}^{16.5}$	10.85/6.56	12.18/5.84	14.04/5.07	16.48/4.33	21.59/3.31

Standard DSC studies

The Fox equation can be used to predict the values of the T_g for a miscible copolymer or blend system as follows [29]:

$$\frac{1}{T_g} = \frac{X_a}{T_{g_a}} + \frac{X_b}{T_{g_b}}$$

(eq. 2)

where T_g is the glass transition temperature of the copolymer, X_a and X_b are the mass fraction of the block A and B, and T_{ga} and T_{gb} are the glass transition temperature for the components A and B. For the present copolymers the T_g of the PDMAEMA is 19°C and the T_g for the PLA homopolymers are indicated in Table 5.

Experimental and predicted values according to equation 2 are shown in Table 5. In this case the variation of the glass transition temperature with the composition is clear. When the PDMAEMA content increases the T_g of the copolymer decreases as predicted by the

Fox equation. Since the predicted and the experimental values are relatively close, it is likely that the copolymers are miscible in the glassy and melt state.

Figure 4 shows DSC heating scans in the temperature region of the glass transition. For all copolymers only one clear glass transition can be observed, another evidence of miscibility.

In view of the DSC and AFM results presented above we can conclude that the block copolymer components are miscible in spite of the weak shoulder shown in the SAXS profile for the DL copolymers. It must be remembered that even miscible block copolymers can exhibit hole correlation effects in the melt that can lead to broad maxima [23]

The influence of the PDMAEMA block on the crystallization of the PLA block is shown in Figure 5. In the DSC cooling and heating scans, we can observe differences between the behavior of the homopolymers and the copolymers. Firstly, the crystallization during cooling (see Figure 5a) disappears for the copolymers, and takes place during the heating process. This cold crystallization is typical for systems with low nucleation density or when the kinetics of crystallization are very slow. [30,31] It is clear that the presence of the covalently linked PDMAEMA blocks are slowing the overall crystallization kinetics of the PLA blocks, as we will corroborate below with isothermal crystallization experiments.

Additionally when we compare homopolymers and copolymers with the same molecular weight (M_n), the melting temperatures (T_m) are shifted to lower values for the copolymers (see Table 6). Since the blocks are miscible in the melt the main effect that is causing the decrease in T_m should be a dilution effect. In other words, the PDMAEMA block acts like a macromolecular solvent surrounding the PLA crystals in the melt. [30-33] Also the fact that the

PLA block is covalently linked to PDMAEMA will affect the crystallization process and in consequence the T_c and T_m values. [33]
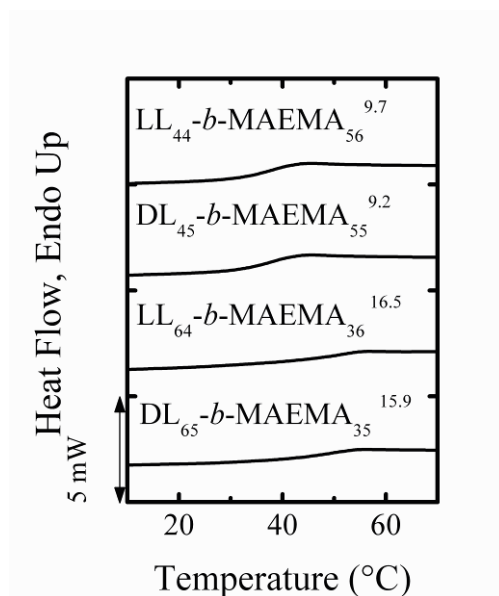

Figure 4: DSC heating scans at 20 °C/min for the PLA-*b*-PDMAEMA block copolymers, detail of the glass transition region.

Table 5: Values for the glass transition temperature of all samples employed: experimentally determined by DSC and predicted by equation 2.

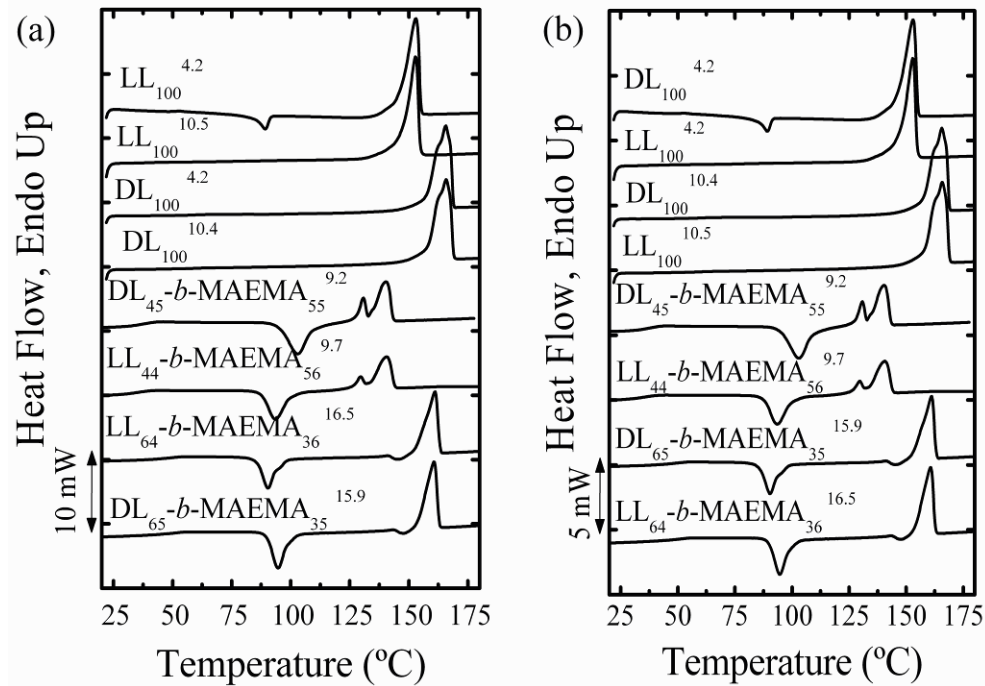| Name	T_g (eq. 2)(ºC)	T_g(DSC) (ºC)
$DL_{100}^{4,2}$	-	46
$LL_{100}^{4,2}$	-	27
DL_{45}-b-$MA_{55}^{9,2}$	31	30
LL_{44}-b-$MA_{56}^{9,7}$	22	28
$DL_{100}^{10,4}$	-	52
$LL_{100}^{10,5}$	-	54
DL_{65}-b-$MA_{35}^{15,9}$	33	37
LL_{64}-b-$MA_{36}^{16,5}$	40	39

Figure 5. DSC cooling (a) and heating (b) scans at 20 °C/min for the PLA-*b*-PDMAEMA block copolymers. Results for homopolymers are also included for comparison purposes.

On the other hand, when the homopolymers and copolymers with different molecular weight are compared amongst themselves, different melting temperatures can be observed. In this case the difference can be attributed exclusively to the M_n of the samples. When the M_n is lower the T_m is lower too, as expected, since this trend usually holds until a maximum M_n value. This value depends on the chemical nature of the polymer; beyond this maximum the T_m remains constant with further increases in M_n. [30,31]

Table 6. Thermal characteristics of the PLA-*b*-PDMAEMA block copolymers obtained by DSC

Sample	cooling scans		heating scans			
	T_c (ºC)	ΔH_c (J/g)	T_c (ºC)	ΔH_c (J/g)	T_m (ºC)	ΔH_m (J/g)
DL$_{100}$[4,2]	94	-34	89	-33	153	59
LL$_{100}$[4,2]	97	-46			153	57
DL$_{45}$-*b*-MA$_{55}$[9,2]			103	-61	140	67
LL$_{44}$-*b*-MA$_{56}$[9,7]			94	-55	141	60
DL$_{100}$[10,4]	105	-45			166	62
LL$_{100}$[10,5]	106	-48			166	61
DL$_{65}$-*b*-MA$_{35}$[15,9]			91	-48	157	52
LL$_{64}$-*b*-MA$_{36}$[16,5]			95	-54	161	56

Isothermal Crystallization

In Figure 6 we show the variation of the inverse of the half-crystallization time ($\tau_{1/2}$) with the isothermal crystallization temperature T_c for the PLA-*b*-PDMAEMA block copolymers. The quantity $1/\tau_{1/2}$ is an experimentally determined value that is proportional to the overall crystallization rate (that includes both nucleation and growth).
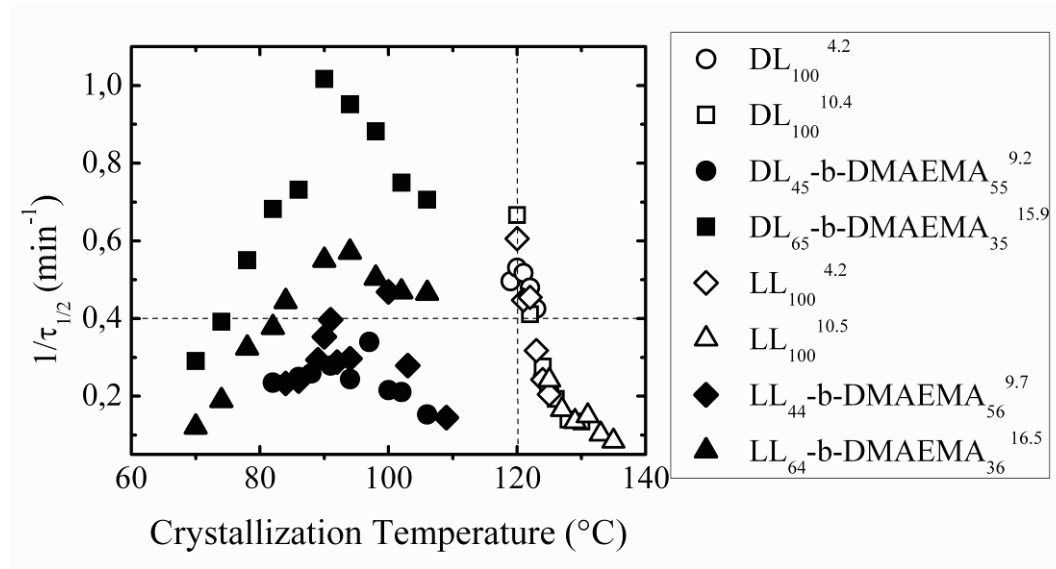

Figure 6. Values of the inverse of half-crystallization time versus the isothermal crystallization temperature for PLA -*b*-PDMAEMA block copolymers

Figure 6 reveals a clear difference between the copolymers and homopolymers. In general the homopolymers crystallize faster than the copolymers. For example if all curves are compared at a fixed temperature (120 °C) this trend is obvious (the copolymer data would have to be extrapolated to be compared with that of the homopolymers at the same temperature). Also, it is possible to observe a maximum in overall crystallization rate with T_c for the copolymers, while for the homopolymers only a decreasing trend with T_c is

observed. In the case of the homopolymers, it was very difficult to determine the crystallization rates at lower T_c values because the samples crystallized during the quenching (at a controlled rate of 60 °C/min) to T_c.

Generally, the copolymers required larger supercoolings for crystallization than the homopolymers. This is an indication of the difficulty encountered by the PLA blocks within the copolymers in order to crystallize as compared to the homopolymers.

Additionally, lower values of T_c are required to obtain the same crystallization rate, as an example, a constant value of $1/\tau_{1/2}$ of 0.4 min^{-1} is indicated in Figure 6 (horizontal dotted line). All these results indicate that the presence of the PDMAEMA block hinders the crystallization of the PLA blocks. When a crystallizable block is covalently linked to another non-crystallizable chain the crystallization process can be retarded. When the melt is homogeneous the PLA block chains have to diffuse out of the melt miscible phase to the crystallizable front, a process that should be easily retarded by the PDMAEMA block.

On the other hand, when the crystallization kinetics of copolymers DL$_{45}$-b-DMAEMA$_{55}$$^{9.2}$ and LL$_{44}$-b-DMAEMA$_{56}$$^{9.2}$ are compared, we find that their overall crystallization rate is almost the same within the range of T_c values employed. The reason for this behavior is that both copolymers crystallize from a homogenous melt. It must be noticed that both sets of PLLA and PDLA homopolymers crystallize with identical crystallization kinetics regardless of their stereochemistry (at identical M_n values)

The composition of the copolymer also has an influence on the crystallization kinetics. [31] The crystallization is slower for the copolymers with a content of approximately 50 % of PDMAEMA than for LL$_{64}$-b-DMAEMA$_{36}$$^{16.1}$. This is probably due to the difficulty

encountered by the PLA chains to diffuse from a homogeneous melt to find the crystal growth front, when their content is 50% or lower, while they are surrounded by melt mixed PDMAEMA chains.

The experimental data obtained during the isothermal crystallizations was analyzed using the Avrami equation, which can be expressed as follows: [21,34]

$$1 - V_c(t - t_0) = \exp\left(-k(t - t_0)^n\right)$$

(eq. 3)

Here t is the experimental time, t_0 is the induction time, V_c is the relative volumetric transformed fraction, n is the Avrami index and k is the overall crystallization rate constant. [21,34]. The procedure employed to perform fits to the Avrami equation was that of Lorenzo et al. [21] The results are shown in Table 7. The Avrami equation represents an excellent fit to the data in the primary crystallization range (i.e., at low relative crystallinity values or low conversion to the semi-crystalline state). Nevertheless a comparison between the experimental and the theoretically predicted values (employing the Avrami fit parameters) of the half crystallization time also indicates that the fits are very good up to 50% conversion since the values are quite similar. In fact, the fittings were very good almost for the entire conversion range, a very unusual occurrence in polymers. This can be demonstrated by comparing the entire experimental DSC isothermal run with that predicted by the Avrami equation in Figure 7 (the calculation was performed by the free Avrami plugin of Lorenzo et al., described in reference 21). Even though the prediction is better for the first half of the DSC isotherm (corresponding roughly to 50% conversion), in the case of the PLA homopolymers, the Avrami equation represents a very good fit for the entire overall crystallization process. For the copolymers, the fit is not as good as for the PLA

homopolymers, but it is still better than for many other polymers (see for instance examples of polyethylenes in ref. 21)

For all the materials examined the values of n indicate the formation of three dimensional structures, namely spherulites, which can be instantaneously nucleated (n values of approximately 3) or sporadically nucleated (values around 4). These results are fully consistent with the experimental observation of spherulites by AFM.

The values of n are higher for the copolymers than the homopolymers in general. This difference is probably due to the fact that nucleation is more sporadic for the copolymers than for the homopolymers. The overall crystallization kinetics are also slower for the copolymers as compared to the homopolymers as discussed previously (Figures 5 and 6) (this is the reason behind the lack of crystallization upon cooling from the melt under non-isothermal conditions, see Figure 5). These results are a consequence of the covalent bond between the PLA chains and the amorphous PDMAEMA chains in the copolymers.

Finally, the values of the overall crystallization rate constant K in Table 7, are fully consistent with the trends exhibited in Figure 6 by the inverse of the half-crystallization times, as expected.
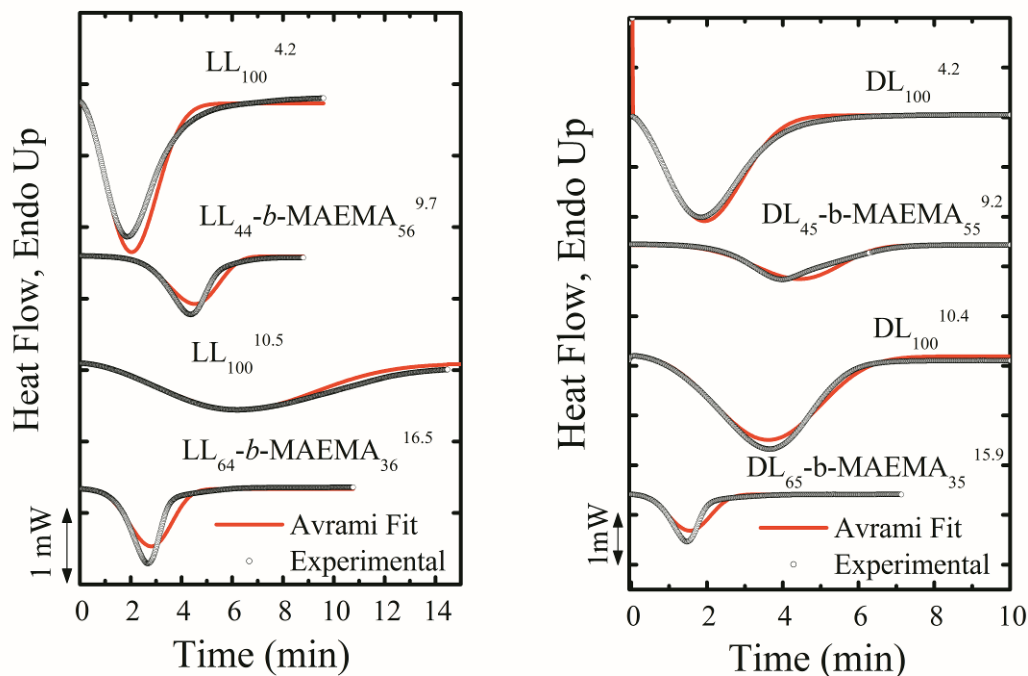
Figure 7. Experimental DSC isotherms and simulated DSC curves by the Avrami equation for (a) $DL_{100}^{4.2}$ (T_c = 122 °C), $DL_{100}^{10.4}$(T_c = 122 °C), DL_{45}-*b*-PDMAEMA$_{55}^{9.2}$ (T_c = 82 °C) and DL_{65}-*b*-PDMAEMA$_{35}^{15.9}$(T_c = 82 °C); (b) $LL_{100}^{4.2}$ (T_c = 122 °C), $LL_{100}^{10.5}$(T_c = 131 °C), LL_{44}-*b*-PDMAEMA$_{56}^{9.7}$ (T_c = 84 °C) and DL_{64}-*b*-PDMAEMA$_{36}^{16.5}$(T_c = 82 °C)

Table 7. Avrami fitting parameters (n, K, $\tau_{1/2\ theo}$), their correlation coefficient R^2 and conversion range employed for the fitting procedure[21]. The experimental value of $\tau_{1/2\ exp}$ is given for comparison purposes.

Sample	T_c (°C)	n	K (min^{-n})	$\tau_{1/2\ theo}$ (min)	$\tau_{1/2exp}$ (min)	R^2	Conversion Range (%)
$DL_{100}^{4.2}$	119	2.6	0.112	2.00	2.02	1.0000	3-20
	120	2.6	0.135	1.86	1.88	1.0000	3-20
	121	2.6	0.130	1.92	1.93	1.0000	3-20
	122	2.6	0.107	2.06	2.08	1.0000	3-20
	123	2.6	0.080	2.29	2.35	1.0000	3-20
	124	2.6	0.021	3.87	4.03	1.0000	3-20
	125	2.6	0.014	4.47	4.68	1.0000	3-20
$DL_{100}^{10.4}$	120	3.0	0.222	1.45	1.50	0.9998	3-20
	122	2.8	0.054	2.49	2.43	0.9999	3-20

23

	124	3.2	0.010	3.66	3.62	1.0000	3-20
	126	3.1	0.004	5.42	5.18	0.9999	3-20
	128	2.8	0.003	7.41	7.13	1.0000	3-20
	130	2.7	0.004	6.98	7.40	0.9998	3-20
	82	4.5	0.001	4.35	4.25	0.9995	5-15
	86	3.9	0.002	4.37	4.00	0.9995	5-15
	88	4.7	0.001	4.07	3.87	0.9992	5-15
	91	4.2	0.002	3.95	3.58	0.9994	5-15
DL_{45}-b-$MA_{55}{}^{9.2}$	94	4.5	0.001	4.29	4.10	0.9991	5-15
	97	4.7	0.004	2.94	2.94	0.9996	5-15
	100	3.8	0.001	5.12	4.63	0.9991	5-15
	102	4.6	0.000	4.91	4.75	0.9992	5-20
	106	4.6	0.000	6.95	6.52	0.9993	5-20
	70	2.9	0.017	3.64	3.43	0.9993	3-20
	74	3.7	0.020	2.61	2.55	0.9996	3-20
	78	3.6	0.074	1.86	1.82	0.9996	3-20
	82	3.4	0.152	1.56	1.47	0.9991	3-20
DL_{65}-b-$MA_{35}{}^{15.9}$	86	4.3	0.161	1.41	1.37	0.9994	5-20
	90	3.8	0.649	1.02	0.98	0.9993	5-20
	94	4.2	0.367	1.08	1.05	0.9993	5-20
	98	4.4	0.356	1.16	1.13	0.9994	5-20
	102	4.8	0.159	1.35	1.33	0.9995	5-20
	106	5.0	0.115	1.43	1.42	0.9995	5-20
	120	2.7	0.187	1.63	1.65	1.0000	3-20
	121	2.7	0.081	2.19	2.23	1.0000	3-20
	122	2.7	0.090	2.15	2.20	1.0000	3-20
$LL_{100}{}^{4.2}$	123	2.7	0.035	3.05	3.15	1.0000	3-20
	124	2.7	0.017	3.90	4.12	0.9999	3-20
	125	2.6	0.013	4.68	4.88	0.9999	3-20
	126	2.7	0.006	5.71	6.17	0.9999	3-20
	125	3.0	0.009	4.28	4.13	0.9999	3-20
	127	2.9	0.003	6.28	6.03	0.9999	3-20
$LL_{100}{}^{10.5}$	129	2.7	0.003	7.42	7.42	1.0000	3-20
	131	2.7	0.004	6.60	6.68	1.0000	3-20
	133	2.8	0.001	9.14	9.73	0.9997	3-20
	135	2.6	0.001	11.26	11.87	0.9997	3-20
	84	5.2	0.000	4.42	4.30	0.9995	5-20
	86	5.1	0.000	4.27	4.18	0.9994	5-20
LL_{44}-b-$MA_{56}{}^{9.7}$	89	4.9	0.002	3.51	3.40	0.9991	5-20
	90	4.8	0.004	2.93	2.83	0.9992	5-20
	91	3.6	0.022	2.59	2.52	0.9992	5-20

	92	5.0	0.001	3.55	3.47	0.9991	5-20
	94	5.2	0.001	3.44	3.37	0.9993	3-20
	100	4.2	0.025	2.21	2.13	0.9990	3-20
	103	5.2	0.001	3.60	3.58	0.9995	5-20
	109	3.1	0.002	7.00	6.90	0.9997	5-20
	70	3.3	0.001	8.62	8.28	0.9997	3-20
	74	3.6	0.002	5.43	5.30	0.9998	3-20
	78	3.1	0.019	3.20	3.08	0.9992	3-20
	82	4.0	0.012	2.78	2.65	0.9991	5-20
LL_{64}-b-MA_{36}[16.5]	84	4.2	0.015	2.46	2.25	0.9995	5-20
	90	2.9	0.073	2.16	1.82	0.9995	5-20
	94	2.8	0.101	2.01	1.75	0.9992	5-20
	98	2.8	0.066	2.30	1.98	0.9991	5-20
	102	3.0	0.045	2.38	2.13	0.9994	5-20
	106	3.2	0.036	2.55	2.15	0.9995	5-20

Poly(D- or L-Lactide)-B-Poly(N.N-Dimethylamino-2-Ethyl Methacrylate) stereocomplexes

Stereocomplexes are formed when the interaction between polymers having dissimilar configurations or tacticities prevails over that between polymers with the same configuration or tacticity. The stereocomplexes between PDLA and PLLA are formed because these crystalline structures are more stable than those obtained with neat PLLA or neat PDLA. The higher stability results from the formation of hydrogen bonds when the PLLA and PDLA crystallize together. [19,36]

The formation of a stereocomplex between PLLA and PDLA can occur as long as the L-lactide and D-lactide sequences coexist in a system. Stereocomplexation can take place in solution, in the bulk state from the melt, during hydrolytic degradation or during polymerization. [36-38] Here, stereocomplexation occurs in solution, due to the solution casting method employed to prepare the samples. In fact, attempts to produce stereocomplexation

in the melt yielded a mixture of stereocomplex and ordinary crystals. Therefore, the solution method was adopted to maximize stereocomplexation.

DSC is frequently used to ascertain the formation of stereocomplexes, since the new crystalline phase is more stable and melts at a higher temperatures than either of its individual components. [35-40] In Figure 8, DSC scans for the stereocomplexes are shown. The melting temperatures of the stereocomplexes are higher than 200 °C in all cases. This result provides evidence for stereocomplex formation. In general, an increase in molecular weight produces a rise in the melting temperature. In addition, the melting temperature of the stereocomplexes formed from the homopolymers is higher than the T_m of the stereocomplexes formed from the copolymers. This indicates that the stereocomplexes from the homopolymers are more stable than those from the copolymers. This is an expected result since the covalent bonding with the PDMAEMA chains probably difficult stereocomplex formation.
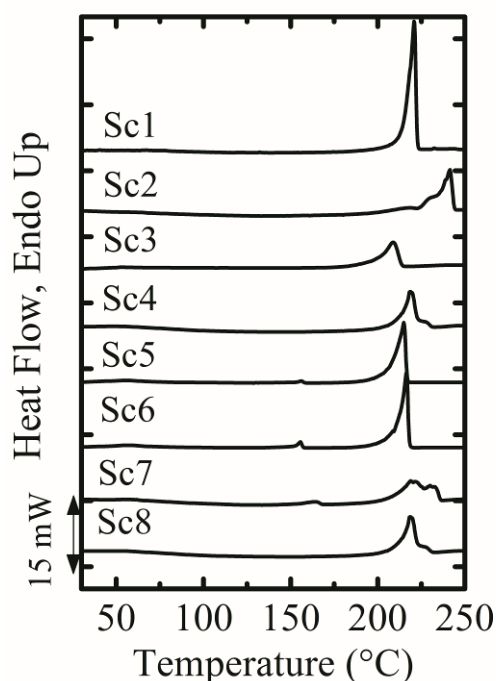
Figure 8. DSC heating scans at 20 °C/min for the PLA/PLA-*b*-PDMAEMA

stereocomplexes indicated

Figure 9 shows AFM images showing the morphology of the particles that result from the formation of stereocomplexes, when the samples were drop coated from chloroform solutions.
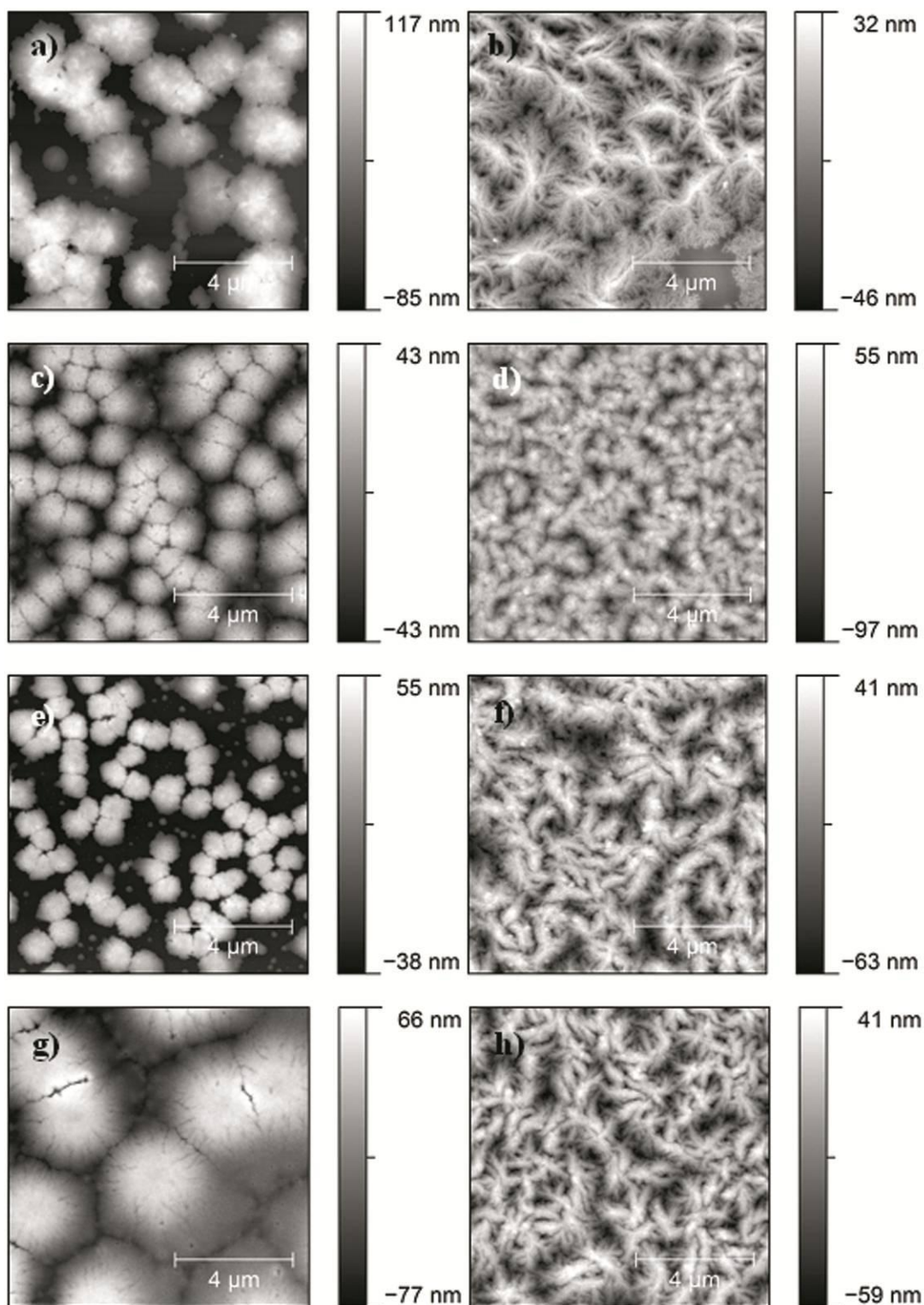
Figure 9. AFM height images of films drop coated from chloroform solution with a
concentration of 1 mg/ml. a) Sc1; b) Sc2; c) Sc3; d) Sc4 e) Sc5; f) Sc6; g) Sc7; h) Sc8

For low molecular weight samples, the particles have a disk-like form. The morphology of the stereocomplexes depends on the molecular weight, concentration of the solution, temperature, evaporation rate of the solvent and DL/LL ratio. [35, 36, 39, 41-43]

However, the morphology of the samples with high molecular weight stereocomplex samples resembles star-like structures (see figure 9 b, d, f, h). It is possible that the evaporation rate of the solvent was too high for these samples and the particles are not fully developed into defined structures. On the other hand, these morphological features could be due to the molecular weight differences in between the samples. It is suggested that parameters such as solvent type, solution concentration and polymer molecular weight are critical to obtain a fully developed particle with well-defined structures. The particles that are shown in figures 9 (b), (d), (f) and (h) could have a transitional morphology.

Beside the molecular weight, the particles obtained for the stereocomplexes Sc3 and Sc4 are smaller than the ones obtained for the other samples. This could be due to the presence of the PDMAEMA block. This block should be outside of the stereocomplex particles and could hinder stereocomplexation in larger particles. On the other hand the stereocomplexes formed by the homopolymer/copolymer mixtures look very similar to the morphologies of stereocomplexes obtained for the homopolymer/homopolymer mixtures. The reason could be that the sterocomplexation in this case is not affected by the PDMAEMA blocks, because the homopolymers can diffuse faster and couple into the stereocomplexes, despite the presence of the PDMAEMA block.

The disk-like shape for the low molecular weight stereocomplexes was confirmed using scanning electron microscopy (SEM) (Figure 10).
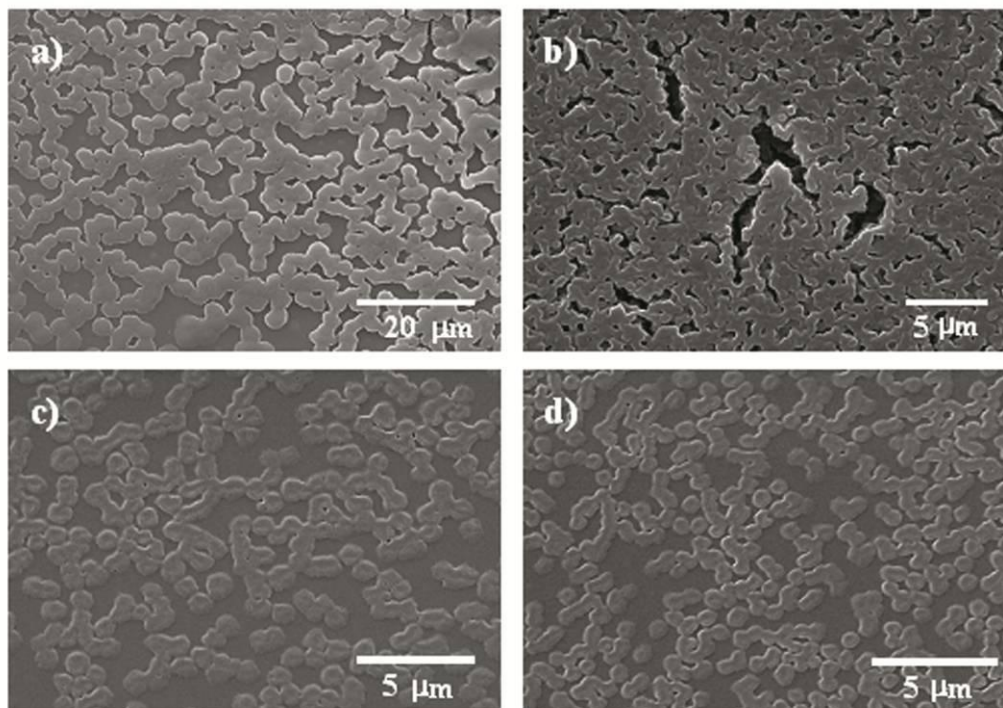

Figure 10. SEM micrographs showing films formed via drop coating techniques of chloroform solution with concentration of 1 mg/ml. a) Sc1; b) Sc3; c) Sc5; d) Sc7

In Figure 10 shows elongated disk-like structures for the low molecular weight stereocomplexes. The micrographs demonstrate copolymer/copolymer stereocomplexes structures with smaller particles than the homopolymer/homopolymer stereocomplexes. Also it is possible to observe a slight depression in the middle of the particles; this feature is common in stereocomplexes with a disk-like structure. [35,36]

CONCLUSIONS

The thermal properties and morphologies of homopolymers, copolymers and stereocomplexes of a series of PLA-based polymers, including copolymers with non-crystalline PDMAEMA, were investigated. The copolymers were found to be miscible when the results of AFM, SAXS and DSC were analyzed together.

In general, the presence of the PDMAEMA hinders PLA nucleation and crystallization. As expected, the composition also had an important influence on the crystallization kinetics, since as the amount of PDMAEMA was increased the crystallization rate was retarded.

The Avrami theory was able to fit the entire isothermal overall crystallization range of the PLA homopolymers, as demonstrated by comparing experimental and simulated DSC isothermal runs. This result is not usual, since the Avrami equation usually holds for the primary crystallization range only. In the case of the PLA blocks the fitting of the DSC isothermal curves was not as good but still much better than the expectation for other polymers based on previous literature. [21]

PLDA and PLLA formed stereocomplexes using equimolar ratios as previously reported in the literature. However, in this work we were able to form stereocomplexes with mixtures of PLA homopolymers and PLA-*b*-PDMAEMA block copolymers as well as between two block copolymers in spite of the presence of the PDMAEMA blocks. The melting point of PLDA/PLLA and PLA/PLA-*b*-PDMAEMA stereocomplexes were higher than those

formed by copolymer mixtures. Therefore, the PDMAEMA block had a disturbing effect on the stereocomplex structure stability. For the low molecular weight stereocomplexes the particles exhibited a conventional disk-shape, on the other hand for high molecular weight samples, the particles displayed unusual star-like shapes.

ACKNOWLEDGEMENTS

REFERENCES

1. Hartmann, M. H. In Biopolymers from Renewable Resources*;* Kaplan, D. L., Ed.; Springer-Verlag: Berlin, **1998**; p 367-411.

2. Garlotta, D. *J Polym Environ* **2001**, *9*, 63-84.

3. De Santis, P.; Kovacs, A. *J Biopolym* **1968**, *6,* 299-306.

4. Ikada, Y.; Jamshidi, K.; Tsuji, H.; Hyon, S. *Macromolecules* **1987**, *20,* 904-906.

5. Pachence, J.; Kohn, J.; Lanza, R. Principles of Tissue Engineering*,* 2nd ed.; Academic Press: San Diego, 2000; p 263.

6. Tsuji, H. *Macromol. Biosci.* **2005**, *5, 569-597.*

7. Yancheva, E.; Paneva, D.; Maximova, V.; Mespouille, L.; Dubois, P.; Manolova, N.; Rashkov, I. *Biomacromolecules* **2007**, *8,* 976-984.

8. Huang, J.; Murata, H.; Koepsel, R. R.; Russel, A. J.; Matjyaszewski, K. *Biomacromolecules* **2007**, *8,* 1396-1399.

9. Spasova, M.; Mespouille, L.; Coulembier, O.; Paneva, D.; Manolova, N.; Rashkov, I.; Dubois, P. *Biomacromolecules* **2009**, *10*, 1217-1223.

10. Spasova, M.; Manolova, N.; Paneva, D.; Dubois, P.; Rashkov, I.; Maximova, V. *Biomacromolecules* **2010**, *11,* 151-159.

11. Castillo, R. V.; Müller, A. J. *Prog Polym Sci* **2009**, *34,* 519-560.

12. Müller, A. J.; Balsamo, V.; Arnal, M. L. In Lecture notes in physics: progress in understanding of polymer crystallization*;* Reiter, G., Strobl, G., Eds.; Springer: Berlin, 2007; Vol. 714, pp 229-259.

13. Müller, A.; Balsamo, V.; Arnal, M. *Adv Polym Sci* **2005**, *190,* 1-63.

14. Yasuniwa, M.; Tsubakihara, S.; Iura, K.; Ono, Y.; Dan, Y.; Takahashi, K. *Polymer* **2006**, *47,* 7554-7563.

15. Vasanthakumari, R.; Pennings, A.J. *Polymer* **1983**, *24,* 175-178.

16. Miyata, T.; Masuko, T. *Polymer* **1998**, *39,* 5515-5521.

17. Iannace, S.; Nicolais, L. *J Appl Polym Sci* **1997**, *64,* 911-919.

18. Tsuji, H.; Miyase, T.; Tezuka, Y.; Saha, S. *Biomacromolecules* **2005**, *6,* 244-254.
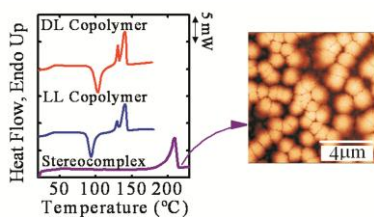
19. Tsuji, H.; Tezuka, Y.; Saha, S.; Suzuki, M.; Itsuno, S. *Polymer* **2005**, *46,* 4917-4927.

20. Xu, J.; Guo, B.H.; Zhou, J.J.; Li, L.; Wu, J.; Kowalczuk, M. *Polymer* **2005**, *46,* 9176-9185.

21. Lorenzo, A.; Arnal, M.; Albuerne, J.; Müller, A. *Polym Test* **2007**, *26*, 222-231.

22. Brandrup, J.; Inmergut, E.; Grulke, E. Polymer Handbook*;* John Wiley and Sons: New York, 1999.

23. Leibler, L. *Macromolecules* **1980**, *13*, 1602-1617.

24. Hamley, I. W. The Physics of Block Copolymers; Oxford University Press: Londres, 1999.

25. Loo, Y.L.; Register, R. A.; Ryan, A. J. *Macromolecules* **2002**, *35*, 2365-2374.

26. Matsen, M.W.; Bates, F.S. *Macromolecules* **1995**, *29,* 1091-1098.

27. Lin, T. T.; Liu, X. Y.; He, C. *Polymer*. **2010**, *51,* 2779-2785.

28. Miyata, T.; Masuko, T. *Polymer* **1997**, *38*, 4003-4009.

29. Gedde, U. W. *Polymer Physics*; Chapman & Hall: London, 1995.

30. Mathot, V. Calorimetry and Thermal Analysis of Polymers*;* Hanse Publishers: New York, **1994**

31. Wunderlich, B. Macromolecular Physics Volumen 2: Crystal nucleation, Growth, Annealing; Academic Press: New York, 1976.

31. Mandelkern, L. Crystallization of Polymers, 2nd ed.; Cambridge University Press: Cambridge, 2002; Vol. 1.

33. Strobl, G. *Prog. Polym. Sci.* **2006**, *31,* 398-442.

34. Avrami, M. *J Chem Phys* **1941**, *9,* 177-184.

35. Hideto, T.; Tezuka, Y.; Saha, K. S.; Suzuki, M.; Itsuno, S. *Polymer* **2005**, *46,* 4917-4927.

36. Ikada, Y.; Tsuji, H. *Macromol Rapid Commun* **2000**, *21,* 117-132.

37. Krouse, S. A.; Schrock, R. R.; Cohen, R. E. *Macromolecules* **1987**, *20,* 904-906.

38. Tsuji, H.; Ikada, Y. *Macromolecules* **1993**, *26,* 6918-6926.

39. Tsuji, H.; Hyon, S.H.; Ikada, Y. *Macromolecules* **1992**, *25,* 2940-2946.

40. Tsuji, H.; Hyu, H.S.; Ikada, Y. *Macromolecules* **1991**, *24 ,* 5651-5656.

41. Narladkar, A.; Balnois, E.; Grohens, Y. *Macromol. Symp.* **2006**, *241,* 34-44.

42. Slager, J.; Brizzolara, D.; Cantow, H. J. *Polym. Adv. Technol.* **2005**, *16 ,* 667-674.

43. Tsuji, H.; Horii, F.; Hyon, S.H.; Ikada, Y. *Macromolecules* **1991**, *24 ,* 2719-2724.

Crystallization and Stereocomplexation Behavior of Poly(D- and L-lactide)-b-poly(*N*,*N*-dimethylamino-2-ethyl methacrylate) Block Copolymers

Rose Mary Michell, Alejandro J. Müller, Mariya Spasova, Philippe Dubois, Stefano Burattini, Barnaby W. Greenland,   Daniel Hermida-Merino, Ian W. Hamley, Nicolas Cheval, Amir Fahmi

Formation of semi-crystalline stereocomplexes of amphiphilic poly(D-lactide)-*b*-poly(*N*,*N*-dimethylamino-2-ethyl methacrylate) (PDLA-*b*-PDMAEMA) and poly(L-lactide)-*b*-poly(*N*,*N*-dimethylamino-2-ethyl methacrylate) (PLLA-*b*-PDMAEMA) and their associated morphology.